Spectrochimica Acta Part A 91 (2012) 272–284

Contents lists available at SciVerse ScienceDirect

Spectrochimica Acta Part A: Molecular and Biomolecular Spectroscopy

journal homepage: www.elsevier.com/locate/saa

Molecular structures of 2-arylaminomethyl-1H-benzimidazole: Spectral, electrochemical, DFT and biological studies

Nour T. Abdel Ghani, Ahmed M. Mansour*

Chemistry Department, Faculty of Science, Cairo University, Gamaa Street, Giza 12613, Egypt

ARTICLE INFO

Article history:
Received 17 November 2011
Received in revised form 15 January 2012
Accepted 30 January 2012

Keywords:
Benzimidazole
NBO
TD-DFT
PCM
Antibacterial

ABSTRACT

In the present work, structural studies on (1H-benzimidazol-2-ylmethyl)-*N*-(4-chloro-phenyl)-amine (L^1) and (1H-benzimidazol-2-ylmethyl)-*N*-(4-iodo-phenyl)-amine (L^2) have been done extensively by a variety of physico-chemical techniques. Optimized geometrical structures, harmonic vibrational frequencies, natural bonding orbital (NBO) analysis, and Frontier molecular orbitals (FMO) were obtained by DFT/B3LYP method. TD-DFT calculations help to assign the electronic transitions. The polarizable continuum model (PCM) fails to describe the experimental chemical shift associated with the NH protons as calculated by applying Gauge-invariant atomic orbital (GIAO) method, but a very good correlation between the theoretical and experimental values was achieved by taking into account the specific solute-solvent interactions. DFT calculations showed a good agreement between the theoretical and observed results. These compounds exhibited a high biological activity through the inhibition of the metabolic growth of the investigated bacteria.

1. Introduction

Benzimidazole derivatives have been proved to be an important group of fungicides with systemic activity and are well known for their pronounced ability to control a large number of fungal diseases [1,2]. Recently, the emergence of resistance to the major classes of antibacterial agents is recognized as a serious health concern. Particularly, multidrugs-resistant strain of Gram-positive bacterial pathogens is a problem of ever-increasing significance, organisms including methicillin-resistant *Staphylococcus aureus* and *Staphylococcus epidermidis*, as vancomycin-resistant *Enterococci* [3]. In addition, substituted benzimidazoles, benzoxazoles and some related heterocycles, which are the structural isosters of nucleotides owing to the fused heterocyclic nuclei in their structures, interact easily with biopolymers and possess potential activity with lower toxicities in the chemotherapeutic approach in man [4,5]. Furthermore, benzimidazoles were used as ligands towards metal ions [6] with a variety of biological molecules including ionheme systems, vitamin B_{12} and its derivatives and several metallo-proteins. These different applications of benzimidazole compounds have attracted many experimentalists and theorists to investigate the structural characteristics of benzimidazole and some of its derivatives.

As a continuation of our recent studies on synthesis, biological activities, structural and theoretical investigations of some substituted benzimidazole [6–8], the main aspect of this study are: (i) synthesis and structural investigation of (1H-benzimidazol-2-ylmethyl)-*N*-(4-chloro-phenyl)-amine (L^1) and (1H-benzimidazol-2-ylmethyl)-*N*-(4-iodo-phenyl)-amine (L^2) (Fig. 1) derivatives by FT-IR, ^{1}H NMR, UV–vis, and elemental analysis. (ii) The molecular geometries, absorption wavelengths, and vibrational spectra of the title compounds were calculated by applying density functional theory (DFT) computations. (iii) The solvent effect on ^{1}H NMR data was introduced by applying the polarizable continuum model (PCM). (iv) HOMO, LUMO, and NBO analysis have been used to give more information regarding charge transfer within the molecule.

2. Experimental

2.1. Synthesis

All chemicals used in the preparation and investigation of the present study were of reagent grade (Sigma). The title compounds were prepared by condensation of equimolar quantities of 2-chloromethylbenzimidazole [7] with 4-chloroaniline (L^1) and 4-iodoaniline (L^2) in ethanol in presence of small amount of sodium iodide for about 24 h [8]. Then, the reaction mixtures were neutralized and the solids were separated by cooling, and re-crystallized from ethanol.

* Corresponding author. Tel.: +20 2 0122211253; fax: +20 2 35728843.
E-mail address: inorganic_am@yahoo.com (A.M. Mansour).

1386-1425/$ – see front matter © 2012 Elsevier B.V. All rights reserved.
doi:10.1016/j.saa.2012.01.080

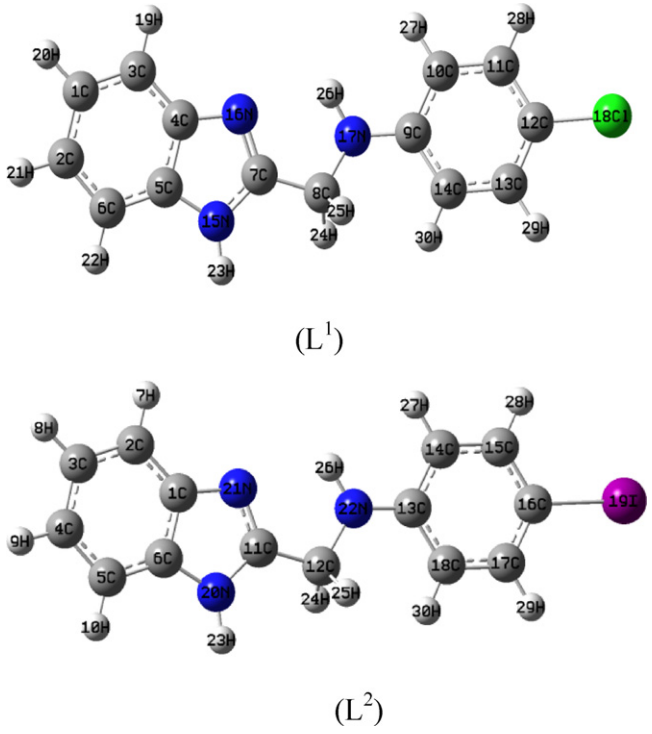

Fig. 1. Optimized structures of the benzimidazoles ($L^{1,2}$).

- Data for L^1 ($C_{14}H_{12}ClN_3$). Color: yellow. MS: $M^+ = 257$ (calcd. 257.72). Anal. calcd. %C, 65.18; %H, 4.66; %Cl, 13.77; %N, 16.30. Found: %C, 65.49; %H, 4.59; %Cl, 13.69; %N, 16.13. FT-IR: 3445 ($\nu(NH)_{sec}$), 3055 (νCH^{ass}/An), 2894 ($\nu CH_2{}^{ass}$), 2827 ($\nu CH_2{}^{ss}$), 1597 (νCC^{ss}/An), and 1309 cm^{-1} ($\nu(C{-}N)_{sec}$). ^1H NMR (DMSO): δ 12.21 (1H, s, benzimidazolic NH); δ 7.47, 7.46, 7.13, and 7.10 (4H, m, benzimidazole ring (Bz)); δ 7.08, 7.06, 6.64, and 6.62 (4H, dd, aniline ring (An)), δ 6.45 (1H, t, NH_{sec}), and δ 4.42 (2H, d, CH_2). UV–vis (ethanol): 204, 222, 250, 274, and 280 nm.
- Data for L^2 ($C_{14}H_{12}IN_3$). Color: yellow. MS: $M^+ = 349$ (calcd. 349.17). Anal. calcd. %C, 48.16; %H, 3.46; %I, 36.34; %N, 12.03. Found: %C, 47.97; %H, 3.69; %I, 35.98; %N, 11.91. FT-IR: 3440 ($\nu(NH)_{sec}$), 3052 (νCH^{ass}/An), 2875 ($\nu CH_2{}^{ass}$), 1691 ($\nu(C{=}N)$), 1588 (νCC^{ss}/An), and 1308 cm^{-1} ($\nu(C{-}N)_{sec}$). ^1H NMR (DMSO): δ 12.25 (1H, s, benzimidazolic NH); δ 7.49, 7.48, 7.14, and 7.12 (4H, m, benzimidazole ring (Bz)); δ 7.36, 7.33, 6.53, and 6.49 (4H, dd, aniline ring (An)), δ 6.50 (1H, t, NH_{sec}), and δ 4.46 (2H, d, CH_2). UV–vis (ethanol): 204, 222, 254, 273 and 280 nm

2.2. Instruments

Elemental microanalyses were performed at the Micro-analytical Center, Cairo University. The analyses were repeated twice to check the accuracy of the analyzed data. The mass spectra were recorded with the aid of a *SHIMADZU QP-2010 plus mass spectrometer* at 70 eV. Infrared spectra were recorded as KBr pellet using *FTIR-460 plus*, *JASCO*, in 4000–200 cm^{-1} region. The ^1H NMR spectra were run at 300 MHz in DMSO-d_6 using *Varian-Mercury VX-300 NMR*. The UV–vis measurements were carried out using automated spectrophotometer UV–vis *SHIMADZU Lambda 4B* using 1 cm matched quartz cells. Cyclic voltammetry measurements were performed using a three-electrode configuration cell connected to "EG&G" scanning potentiostat model 372. A Pt disc was used as working electrode and a Pt wire as auxiliary electrode. The reference electrode was Ag/AgCl electrode adjusted to 0.00 V versus SCE. Sample solutions (50 ml) of 10^{-3} M concentration in acetonitrile with 0.1 M $NaClO_4{\cdot}H_2O$ as supporting electrolyte were used for the measurements. A potential range of +2000 to −2000 mV, with a scan rate of 100 mV s^{-1} was used.

2.3. Computational calculations

The gas phase geometries of (1H-benzimidazol-2-ylmethyl)-*N*-(4-chloro-phenyl)-amine (L^1) and (1H-benzimidazol-2-ylmethyl)-*N*-(4-iodo-phenyl)-amine (L^2) in the ground state were optimized by DFT/B3LYP method [9] using 6-31G(d) basis set for L^1 and SDD for L^2 using *GAUSSIAN03* [10] program. The main reason for choosing the SDD basis set is its inclusion of relativistic effect that is essential for heavy elements. The optimized geometries were verified by performing a frequency calculation. Frontier molecular orbitals (FMO) were performed at the same level of theory. Vibrational modes were analyzed using *GAUSSVIEW* software [11]. Based on the optimized geometries, the electronic spectra of the studied compounds were obtained by using time-dependent density functional theory (TD-DFT) [12] method. Net atomic charges had been obtained by the natural bond orbital (NBO) analysis of Weinhold and Carpenter [13]. The ^1H NMR chemical shifts were computed at the B3LYP/6-311 + G(2d,p) (L^1) and SDD (L^2) level of theory in the gaseous state by applying Gauge-invariant atomic orbital (GIAO) approach [14] and the values for the ^1H, isotropic were referenced to TMS, which was calculated at the same level of theory. The effect of solvents (DMSO, and $CHCl_3$) on the theoretical NMR parameters was performed using the polarizable continuum model (PCM).

2.4. Biological activity studies

The antimicrobial activities of the test samples were determined by means of a modified Kirby-Bauer disc diffusion method [15] under standard conditions using Mueller-Hinton agar medium (tested for composition and pH), as described by NCCLS [16]. The antimicrobial activities were carried out using culture of *Bacillus subtilis*, *S. aureus*, and *Streptococcus faecalis* as Gram-positive bacteria and *Escherichia coli*, *Pseudomonas aeruginosa*, and *Neisseria gonorrhea* as Gram-negative bacteria. The solution of 100 mg/ml of each compound (studied compounds and standard drug *Tetracycline*) in DMSO was prepared for testing against bacteria. Centrifuged pelletes of bacteria from a 24 h old culture containing approximately 10^4–10^6 CFU (colony forming unit) per ml were spread on the surface of Mueller-Hinton agar plates. Then the wells were seeded with 10 ml of prepared inocula to have 10^6 CFU/ml. Petri plates were prepared by pouring 100 ml of seeded nutrient agar. DMSO (0.1 ml) alone was used as control under the same conditions for each microorganism, subtracting the diameter of inhibition zone [17] resulting with DMSO, from that obtained in each case. The antimicrobial activities could be determined as a mean of three replicates.

3. Results and discussion

3.1. Vibrational analysis

The theoretical IR spectra of the investigated compounds ($L^{1,2}$) were obtained at DFT/B3LYP level of theory using 6-31G(d) and SDD basis sets, respectively (Fig. 2). All band assignments are presented in Tables 1 and 2. It is well known that the calculated harmonic frequencies by DFT method are usually higher than the corresponding experimental quantities due to the electron correlation approximate treatment, anharmonicity effects and basis set deficiencies, etc. [18]. To compensate these shortcomings, scale factors were introduced and an explanation of this approach was discussed [19]. Two different methods were applied: (i) uniform scaling [19], the scaling factor is 0.963 for B3LYP/6-31G(d) and 0.970 for B3LYP/SDD

Table 1
Observed and calculated selected frequencies (cm^{-1}) and assignments of the fundamental modes for (1H-benzimidazol-2-ylmethyl)-*N*-(4-chloro-phenyl)-amine (L^1).

No.	Exp. frequency	Calculated un-scaled frequency B3LYP	Scaled frequency uniform scaling	Scaled frequency linear regression scaling	Vibrational assignments
		B3LYP/6-31G(d)			
1		3649	3513	3515	νNH^{ss}/Bz
2	3445	3562	3430	3431	νNH^{ss}/An
3		3221	3101	3102	νCH^{ss}/An
4		3219	3099	3101	νCH^{ass}/An
5		3219	3099	3101	νCH^{ss}/Bz
6		3209	3090	3091	νCH^{ass}/Bz
7		3204	3085	3086	νCH^{ass}/An
8		3197	3078	3079	νCH^{ass}/Bz
9		3188	3070	3071	νCH^{ass}/Bz
10	3055	3185	3067	3068	νCH^{ass}/An
11	2894	3000	2889	2890	$CH_2{}^{ass}$
12	2827	2945	2836	2837	$CH_2{}^{ss}$
13		1683	1620	1621	$\nu CC/Bz + \nu CN/Bz + \beta NH^{sc}/Bz$
14	1597	1666	1604	1604	$\nu CC/An$
15		1642	1581	1581	$\nu CC/Bz + \beta NH/Bz$
16		1631	1570	1571	$\nu CC/An + \beta NH^{sc}/An$
17		1595	1535	1536	$\nu CC/Bz + \beta NH/Bz + \beta NH/An + \delta_s CH_2 + \nu CN/Bz$
18	1501	1559	1501	1501	$\beta NH/An + \delta_s CH_2 + \nu CC/An$
19		1544	1486	1487	$\beta NH/An + \delta_s CH_2$
20		1538	1481	1481	$\nu CC/An + \beta NH/An + \omega CH_2$
21	1431	1497	1441	1442	$\nu CC/Bz$ (boat shape)
22		1470	1415	1415	$\delta_s CH_2 + \nu C{-}NH/Bz$
23		1449	1395	1395	$\nu CC/Bz + \nu CC/An + \beta NH/Bz + \beta NH/An$
24		1425	1372	1372	$\beta NH/Bz + \nu CC/Bz + \beta NH/An + \omega CH_2$
25		1369	1318	1318	$\nu CC/An + \beta NH/Bz + \omega CH_2$
26	1309	1367	1316	1316	$\nu CC/An + \nu C{-}NH/An$
27		1337	1287	1287	$\beta CH/An$
28	1270	1333	1283	1283	$\beta CH/Bz + \beta CH/An + \omega CH_2$
29		1290	1242	1242	$\beta NH/An + \omega CH_2$
30		1258	1211	1211	$\tau CH_2 + \beta NH/Bz + \beta CH/An$
31		1248	1201	1202	τCH_2
32	1184	1216	1171	1170	$\beta CH^{ss,sc}/An + \beta NH/Bz$
33		1207	1162	1162	$\beta CH^{ss,sc}/An + \beta NH/Bz + \beta CH^{ss,sc}/Bz$
34		1183	1139	1138	$\beta CH^{ss,sc}/Bz$
35	1115	1165	1121	1121	$\beta CH^{ss,sc}/An + \nu CH_2{-}NH/An + \beta NH/Bz$
36		1144	1101	1101	$\beta CH^{ss,sc}/Bz$
37	1088	1136	1093	1093	$\beta CH^{ss,sc}/An + \nu CH_2{-}NH/An$
38	1019	1046	1007	1006	$\beta CH/Bz + \rho CH_2$
39		1042	1003	1003	ρCH_2
		674	649	648	
40		1024	986	985	Rtorsion/Bz
41		1020	982	981	Rtrigd/An
42	917	975	938	938	$\gamma CH/Bz$
		931	896	896	
		862	830	829	
		758	729	729	
43	806	942	907	906	$\gamma CH/An$
	744	931	896	896	
		825	794	793	
		808	778	777	
		704	677	677	
44		911	877	876	Rtorsion/Bz
45	657	669	644	643	$\nu C{-}Cl$
46		648	624	623	Rtrigd/An
47	613	631	607	607	Rtrigd/Bz
48	438	443	426	425	$\gamma NH/Bz$
49	499	579		556	$\gamma NH/An$

R: ring; ss: symmetric stretching; ass: asymmetric stretching; ν: stretching; β: in-plane bending; γ: out-of-plane bending; δ_s: scissoring; ω, wagging; τ: twisting; ρ: rocking; trig: trigonal; trigd: trigonal deformation.

(ii) linear regression method [19], in this method, the plot of the calculated frequencies versus their experimental values resulted in a straight line, whose equation was used to correct the calculated frequencies ($\nu_{calcd.}$) (Fig. 3).

Benzimidazole derivatives ($L^{1,2}$) have a strong intermolecular hydrogen bond [8], between the pyridine-type nitrogen, and the benzimidazolic NH group, which makes the IR spectra show a broad absorption band in the region 3500–2200 cm^{-1}. It is not surprising to find this effect since benzimidazole and imidazole derivatives, possessing free imino hydrogen, are known to be capable of associating through hydrogen bond formation [20]. The scaled values at 3513 and 3569 cm^{-1} are assigned to the stretching mode of the benzimidazolic NH group in the benzimidazoles ($L^{1,2}$). The presence of a sharp band at 3445 (L^1) and 3440 cm^{-1} (L^2) indicated the existence of free secondary amino group (NH_{sec}) and these values deviate from the theoretically scaled modes, 3430 and 3471 cm^{-1}, respectively. This discrepancy may be justified on the basis that the calculations were performed on a single molecule in the gaseous state, whereas packing molecules with intermolecular interactions are treated in the experimental measurements.

Table 2
Observed and calculated selected frequencies (cm^{-1}) and assignments of the fundamental modes for (1H-benzimidazol-2-ylmethyl)-*N*-(4-iodo-phenyl)-amine (L^2).

No.	Exp. frequency	Calculated un-scaled frequency	Scaled Frequency Uniform scaling	Scaled frequency linear regression scaling	Vibrational assignments
		B3LYP/SDD			
1		3680	3569	3543	νNH^{ss}/Bz
2	3440	3579	3471	3446	νNH^{ss}/An
3		3239	3141	3118	νCH^{ss}/Bz
4		3234	3136	3113	νCH^{ss}/An
5		3230	3133	3109	νCH^{ass}/An
6		3225	3128	3105	νCH^{ass}/Bz
7		3210	3113	3090	νCH^{ass}/Bz
8		3209	3112	3089	νCH^{ass}/An
9		3198	3102	3079	νCH^{ass}/Bz
10	3052	3194	3098	3075	νCH^{ass}/An
11	2875	2989	2899	2877	$CH_2{}^{ass}$
12		2967	2877	2856	$CH_2{}^{ss}$
13	1691	1675	1624	1612	$\nu CC/Bz + \nu CN/Bz$
14	1588	1653	1603	1591	$\nu CC/An$
15		1635	1585	1573	$\nu CC/Bz + \beta NH^{sc}/Bz$
16		1612	1563	1551	$\nu CC/An + \beta NH^{sc}/An$
17		1580	1532	1520	$\nu CC/Bz + \beta NH/Bz + \beta NH/An + \delta_s CH_2$
18		1547	1500	1488	$\beta NH/An + \delta_s CH_2$
19	1494	1533	1487	1475	$\beta NH/An + \delta_s CH_2$
20		1516	1470	1459	$\nu CC/An + \beta NH/An + \omega CH_2$
21		1513	1467	1456	$\nu CC/Bz + \nu CN/Bz$
22	1425	1480	1435	1424	$\nu CC/Bz$
23		1446	1402	1391	$\delta_s CH_2 + \nu C{-}NH/Bz$
24		1433	1390	1379	$\nu CC/Bz + \nu CC/An + \beta NH/Bz$
25		1427	1384	1373	$\nu CC/Bz + \nu CC/An + \beta NH/An + \omega CH_2$
26	1308	1377	1335	1325	$\nu CC/An + \nu CN/Bz$
27		1340	1299	1289	$\beta CH/An$
28	1268	1325	1285	1275	$\beta CH/An + \beta CH/Bz + \beta NH/An$
29	1223	1290	1251	1241	$\beta CC/Bz + \beta CH/Bz$
30		1249	1211	1201	τCH_2
31		1248	1210	1201	$\beta CH/Bz + \beta NH/Bz$
32		1229	1192	1182	$\beta CH^{ss,sc}/An + \beta NH/Bz$
33		1193	1157	1148	$\beta CH^{ss,sc}/Bz$
34	1119	1166	1131	1122	$\beta CH^{ss,sc}/An + \nu CH_2{-}NH$
35		1140	1105	1096	$\beta CH^{ss,sc}/Bz$
36		1134	1099	1091	$\beta CH^{ss,sc}/An + \nu CH_2{-}NH$
37	1018	1049	1017	1009	ρCH_2
		676	655	650	
38	992	1034	1002	994	Rtorsion/Bz
39	877	1024	993	985	$\gamma CH/Bz$
		983	953	945	
		897	870	862	
		799	775	768	
		786	762	756	
40		1009	978	970	Rtorsion/Bz
41		1004	973	966	Rtrigd/An
42	801	995	965	957	$\gamma CH/An$
	743	976	946	939	
	497	851	825	818	
		836	810	804	
		722	700	694	
		521	505	500	
		424	411	407	
43		908	880	873	Rtrigd/Bz
44		647	627	622	Rtrigd/An
		626	607	601	Para deformation of aniline ring
45	575	603	584	579	$\gamma NH/Bz$
46		562	545	540	$\gamma NH/An$
47		302	292	289	$\nu C{-}I$

R: ring; ss: symmetric stretching; ass: asymmetric stretching; ν: stretching; β: in-plane bending; γ: out-of-plane bending; δ_s: scissoring; ω: wagging; τ: twisting; ρ: rocking; trig: trigonal; trigd: trigonal deformation.

The band at 1691 cm^{-1} in the p-I derivative (L^2) is assigned to $\upsilon(C{=}N)$ [21] and is slightly deviated from the un-scaled calculated mode, 1674 cm^{-1}. It is possible to notice that in the latter range, the scaling is not necessary, as already pointed by Agathabay et al. [22] and Miranda et al. [23]. However, in the p-Cl derivative, this band is overlapped with the aromatic C=C bands in the same region under the effect of the intermolecular hydrogen bond. The theoretical value at 1683 cm^{-1} (L^1) is assigned to $\upsilon(C{=}N)$. Theoretically, the benzimidazoles $L^{1,2}$ give rise to eight C—H aromatic stretching mode of vibration corresponding to the presence of eight aromatic C—H bonds as shown in Tables 1 and 2.

For assignment of CH_2 group frequencies theoretically, six fundamentals can be associated to each CH_2 group [24]. The bands observed at 2889 and 2836 cm^{-1} in L^1 derivative are ascribed to CH_2 asymmetric and symmetric stretching vibration. Infrared bands established at 1535, 1481, 1201, and 1003 cm^{-1} are attributed to

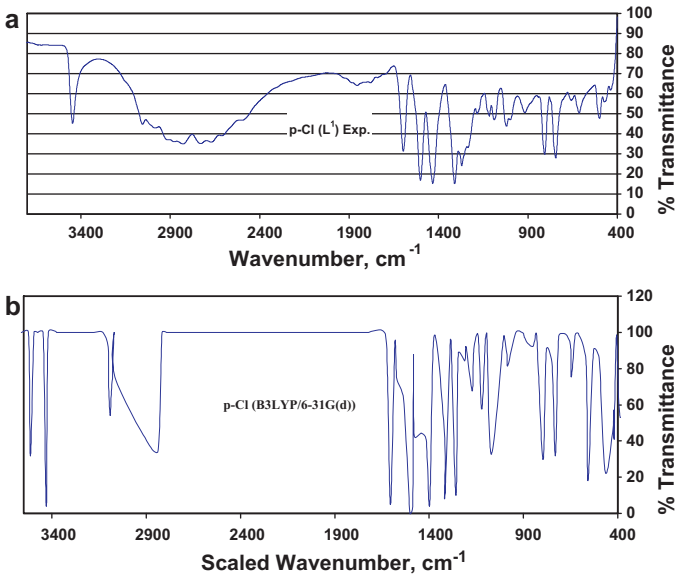

Fig. 2. Experimental and theoretical (B3LYP/6-31G(d)) FT-IR spectra of benzimidazole (L^1).

$\delta_s CH_2$ (scissoring), ωCH_2 (wagging), τCH_2 (twisting), and ρCH_2 (rocking) vibration modes, respectively. For benzimidazole (L^2), the IR bands observed at 2889, 2877, 1532, 1470, 1211, and 1017 cm^{-1} are unambiguously assigned to CH_2^{ass}; CH_2^{ss}, $\delta_s CH_2$, ωCH_2, τCH_2, and ρCH_2, respectively. Other vibration modes are tabulated in Tables 1 and 2. The RMS error of the frequencies between the un-scaled and experimentally observed in benzimidazole (L^1) was found to be 86 cm^{-1}. After scaling, the RMS error is found to be 13 cm^{-1}.

3.2. ^1H NMR spectral analysis

In order to provide an unambiguous assignment of ^1H NMR spectra of the studied compounds, we undertook a series of NMR calculations using GIAO approximation, and the results of these calculations are shown in Table 3. Two models have been used for assessing the influence exerted by solvent on the NMR spectra of the given compound. The first is the polarizable continuum model (PCM) [25] provided by *GAUSSAIN03* with DMSO and chloroform as solvents (UFF radii were used to obtain molecular cavity). Molecular clusters, as microscopic model for the environment, have also been used by placing two DMSO molecules near the NH groups in the studied compounds. In these two models, the ^1H NMR chemical shifts were computed at the DFT/B3LYP/6-311 + G(2d,p) and SDD levels of theory for the benzimidazoles ($L^{1,2}$), respectively. Results of linear regression fit between experimental and calculated chemical shifts (^1H) performed for the structures tested are also included in Table 3.

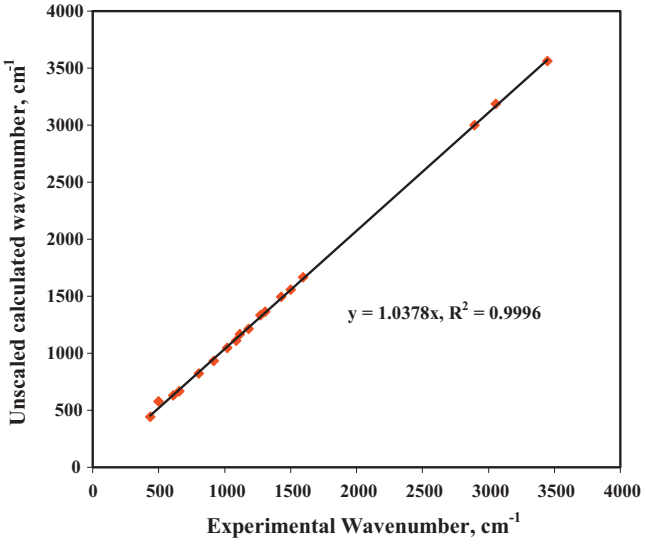

Fig. 3. The linear regression between the experimental and the theoretical DFT predicted wavenumbers (cm^{-1}) for the p-Cl benzimidazole derivative (L^1) using B3LYP/6-31G(d) method.

Experimentally, the benzimidazoles ($L^{1,2}$) showed a broad singlet signal at 12.21 and 12.25 ppm [6], respectively, due to the benzimidazolic NH proton (Fig. 4). The triplet signal at 6.45 and 6.50 ppm is attributed to the secondary amino group, whereas the doublet signal at 4.42 and 4.46 ppm is assigned to the CH_2 protons in $L^{1,2}$. For benzimidazole L^1, the protons of the aniline ring give rise to four-line pattern at 6.64 and 6.62 ppm for protons in the ortho-position with respect to secondary amino group, whereas the protons at 7.08 and 7.06 ppm are assigned to aromatic protons in the ortho-position with respect to chloro atom. The signals at 7.47, 7.46, 7.13, and 7.10 ppm are assigned to the aromatic protons of the benzimidazole ring. Similar, L^2 has the same assignments for the aromatic protons as L^1 at 7.36, 7.33, 6.53, 6.49 and 7.49, 7.48, 7.14, 7.12, respectively.

The ^1H chemical shifts of all protons in the investigated compounds except the imidazolic and the secondary amino protons, (H23 and H26) (L^1) and (H22 and H25) (L^2), are in a good agreement with the theoretically computed values as calculated by the PCM model (Table 3). The regression coefficient between the calculated and the experimental chemical shifts is improved in presence of DMSO as a solvent rather than in the gaseous state. However, the chemical shifts of the NH protons remain unacceptable apart from the experimental values, being obviously that the chemical shifts associated with these protons are not correctly described by continuum model. Thus, it is clear that the PCM model fails in reproducing the experimental findings for the hydrogen-bonded protons and specific solute–solvent interactions are expected to completely explain the ^1H NMR spectra of the studied compounds [26]. For this purpose, we optimized and then calculated the NMR spectra of the p-Cl and p-I molecules with two DMSO molecules. As shown in Table 3, the chemical shift of the benzimidazolic NH proton is in a very good agreement with the theoretical computed value revealing that some sort of interaction occurs between the studied compound and solvent molecules and this will be confirmed later by studying the electronic spectra of these compounds in DMSO. Therefore, the hydrogen bonding interaction of these compounds, is better reproduced by the second model rather than using the polarizable continuum model (PCM) solvation model.

3.3. Electronic absorption

3.3.1. Band assignment

The electronic spectra of the benzimidazoles ($L^{1,2}$) displayed five absorption bands in ethanol. The first two bands at 204 and 222 nm may be assigned to medium and low energy π–π^* transitions within the phenyl rings of the aniline and benzimidazole moieties, respectively [27]. In benzimidazole ring, three kinds of transitions are possible: (i) n–π^*, (ii) π–π^*, and (iii) charge-transfer. However, it is well established that the n–π^* transition is not observed in the benzimidazole compounds, although the system has a lone pair of electrons on the tertiary nitrogen atom [28]. Therefore, the bands at 250, 274, and 280 nm (L^1) and 254, 273 and 280 (L^2) may be assigned to π–π^* transitions in the benzimidazole ring. Moreover, the lowest energy bands in the studied compounds appear doublet due to the presence of a tautomeric

Table 3
Experimental and calculated ^{1}H NMR chemical shifts for the title compounds (L^{1-2}).

L^1						L^2					
Atom	δ Calcd.				δ Exp.	Atom	δ Calcd.				δ Exp.
	Gaseous	$CHCl_3$	DMSO	L^1-DMSO[a]			Gaseous	DMSO	$CHCl_3$	L^2-DMSO[a]	
H_{19}	8.15	8.09	8.08	7.87	7.47	H_{18}	8.25	8.24	8.26	7.78	7.15
H_{20}	7.61	7.58	7.60	7.49	7.10	H_{19}	7.75	7.89	7.85	7.48	7.14
H_{21}	7.59	7.62	7.66	7.57	7.13	H_{20}	7.75	7.95	7.89	7.51	7.49
H_{22}	7.63	7.81	7.92	7.72	7.46	H_{21}	7.51	7.96	7.81	7.56	7.48
H_{23}	8.16	8.76	9.01	13.03	12.21	H_{22}	7.56	8.57	8.26	12.22	12.25
H_{24}	4.42	4.66	4.76	4.59	4.42	H_{23}	4.14	4.44	4.34	4.38	4.46
H_{25}	4.42	4.46	4.51	4.20	4.42	H_{24}	4.14	4.44	4.34	3.76	4.46
H_{26}	5.62	5.62	5.62	7.33	6.45	H_{25}	5.88	5.90	5.92	7.14	6.50
H_{27}	7.02	7.16	7.21	7.67	7.08	H_{26}	6.98	7.24	7.17	7.99	7.36
H_{28}	7.51	7.40	7.42	7.37	6.64	H_{27}	7.50	7.60	7.57	7.31	7.33
H_{29}	7.38	7.60	7.64	7.48	7.06	H_{28}	7.48	7.64	7.58	7.39	6.53
H_{30}	6.33	6.73	6.84	6.76	6.62	H_{29}	6.37	6.84	6.68	6.69	6.49
R^2	0.9326	0.9706	0.9759	0.9711		R^2	0.8777	0.9152	0.9052	0.9161	

[a] These values were obtained after optimization of $L^{1,2}$·2DMSO in the gaseous state.

structure [29]. This phenomenon is supported by comparing our spectra with the spectrum of 1-methyl-2-phenyl-benzimidazole [28], where this fine structure is lost. To explain the effect of the substituent on the absorption spectra of the benzimidazoles ($L^{1,2}$), the unsubstituted derivative [30], which has five absorption bands in ethanol at 204, 222, 242, 274 and 280 nm was taken as a reference. The introduction of electron-attracting substituents (Cl or I) causes a red shift of the band at 242 nm on going from p-Cl to p-I derivative.

The absorption spectra of the benzimidazoles ($L^{1,2}$) were observed in solvents of different polarities and hydrogen bond formation tendency, cyclohexane, DMSO, DMF, dioxane, acetonitrile, 2-propanol, and ethanol (Fig. 5). The two bands at 274 and 280 nm in the cylcohexane (reference solvent) are slightly blue shifted in ethanol and 2-propanol (hydrogen-bonding solvents) suggests that the benzimidazole derivatives are acting as a proton acceptor [31] at the pyridine-type nitrogen. However, the latter bands are red-shifted in DMF and DMSO (hydrogen bond acceptor solvents) due to an almost proton transfer from the solute molecules to these solvents. The values of the observed transition energies (E_{obs}) and oscillator strengths (f_{obs}) of all the bands in the electronic spectra of the title compounds in different solvents were calculated [27] and tabulated in (Supplementary material, Table S1). Application of dielectric relation [27] to the band at 250 (L^1) and 254 nm (L^2) did not give a linear relation indicating that the spectral shifts are not governed solely by the dielectric effect of the solvents. Thus, the so-called specific solute-solvent interaction is the main controlling factor in determining the band position.

The lowest 10 singlet-to-singlet spin-allowed excitation states were taken into account for the calculation of the electronic absorption spectra by using TD-DFT method. The calculated energy of excitation states and transition oscillator strength (f) (only $f > 0.005$ is listed) of the title compounds is taken into consideration. The absorption spectrum was simulated using *GAUSSSUM* software [32] based on the obtained TD-DFT results. Each excited state was interpolated by a Gaussian convolution with the full-width at half-maximum (FWHM) of 3000 cm^{-1}. The theoretical UV–vis spectrum of the benzimidazole (L^1) is characterized by nine electronic transitions at 209, 211, 214, 227, 233, 235, 245, 270, and 297 nm. The lowest energy electronic transition at 297 nm (4.17 eV) characterizes the transition from HOMO to LUMO, while that at 270 nm (4.59 eV) is assigned mainly to HOMO → LUMO + 1 (91%). Moreover, the excitation energy at 245 nm (5.05 eV) is contributed from the transitions between HOMO-1 and LUMO (21%)/LUMO + 2 (7%)/LUMO + 3 (10%) in addition to HOMO-2 → LUMO (54%) transition. The electronic transitions at 235 nm (5.26 eV) are connected with HOMO → LUMO + 2 (68%), and HOMO → LUMO + 3 (28%). The electronic transitions between HOMO and LUMO + 2 (7%)/LUMO + 3 (4%), HOMO-1 and LUMO (55%)/LUMO + 3 (3%) in addition to HOMO-2 and LUMO (22%)/LUMO + 3 (3%) are attributed to 233 nm (5.31 eV). The highest energy transitions at 211 (5.87 eV) and 214 nm (5.79 eV) are assigned to HOMO-3 → LUMO (96%) and HOMO-1 → LUMO + 1 (96%), respectively. The excitation energy at 209 nm (5.92 eV) is assigned to HOMO-2 → LUMO + 1 (24%), and HOMO → LUMO + 5 (71%).

On the other hand, the theoretical UV–vis spectrum of the benzimidazole (L^2) is characterized by five electronic transitions at 233, 240, 249, 253, and 283 nm. The lowest excitation energy at 283 nm (4.37 eV) characterizes the transitions from HOMO → LUMO + 2 (93%) and HOMO-5 → LUMO + 4 (4%), while the electronic transition at 253 nm (4.90 eV) is due to HOMO → LUMO + 3 (95%) and HOMO → LUMO + 4 (2%). The electronic transitions between HOMO and LUMO + 4 (3%), HOMO-1 and LUMO + 3 (20%)/LUMO + 4 (2%) in addition to HOMO-2 → LUMO (67%) are attributed to 249 nm (4.99 eV). The excitation energy at 240 nm (5.17 eV) is assigned mainly to HOMO → LUMO + 4 (67%). The highest energy transition at 233 (5.30 eV) is due to HOMO-1 → LUMO (73%), HOMO → LUMO + 4 (12%) and HOMO-2 → LUMO + 3 (8%) transitions.

3.3.2. *Electronic absorption spectra in solutions of varying pH*

The absorption spectra of 3×10^{-5} M solutions of $L^{1,2}$ compounds in 20% (v/v) ethanolic solutions of varying pH values were scanned in the UV–vis range. p-Cl derivative (L^1) is neutral over the entire pH range 4.5–8.2 and possesses a clear isosbestic point in the acidic medium at 213 nm as shown in Fig. 6. The bands located at 250, 274 and 280 nm in ethanol are blue shifted to 243, 269 and 275 nm at pH 2 (H_2L^{2+}). With increasing the pH, these bands remain in their new positions with the appearance of shoulder at 279 nm at pH 5. Between pH 6 and 12, these bands are red shifted to 247, 273, and 279 nm, accompanied by a variation in the absorbance values according to the presented species (L^- and L^{2-}). p-I derivative (L^2) has the same behavior as p-Cl compound with a clear isosbestic point in the acidic medium at 213 nm. The pH-absorbance changes [33] were utilized to calculate the acid dissociation constants. Four pK_a values were reported for the investigated compounds. The first pK_a value 2.49 ± 0.02 for the p-Cl derivative (L^1) is assigned to the deprotonation of the protonated secondary amino group, while the second pK_a 4.42 ± 0.03 may be attributed to the deprotonation of the protonated pyridine type nitrogen [34]. The third pK_a 8.43 ± 0.02 is accounted for the ionization of the NH_{sec} group, while the fourth pK_a 11.42 ± 0.01 is attributed to ionization of the imidazolic proton [33]. On the other hand, the pK_a values at 2.71 ± 0.01, 5.06 ± 0.04, 7.84 ± 0.03

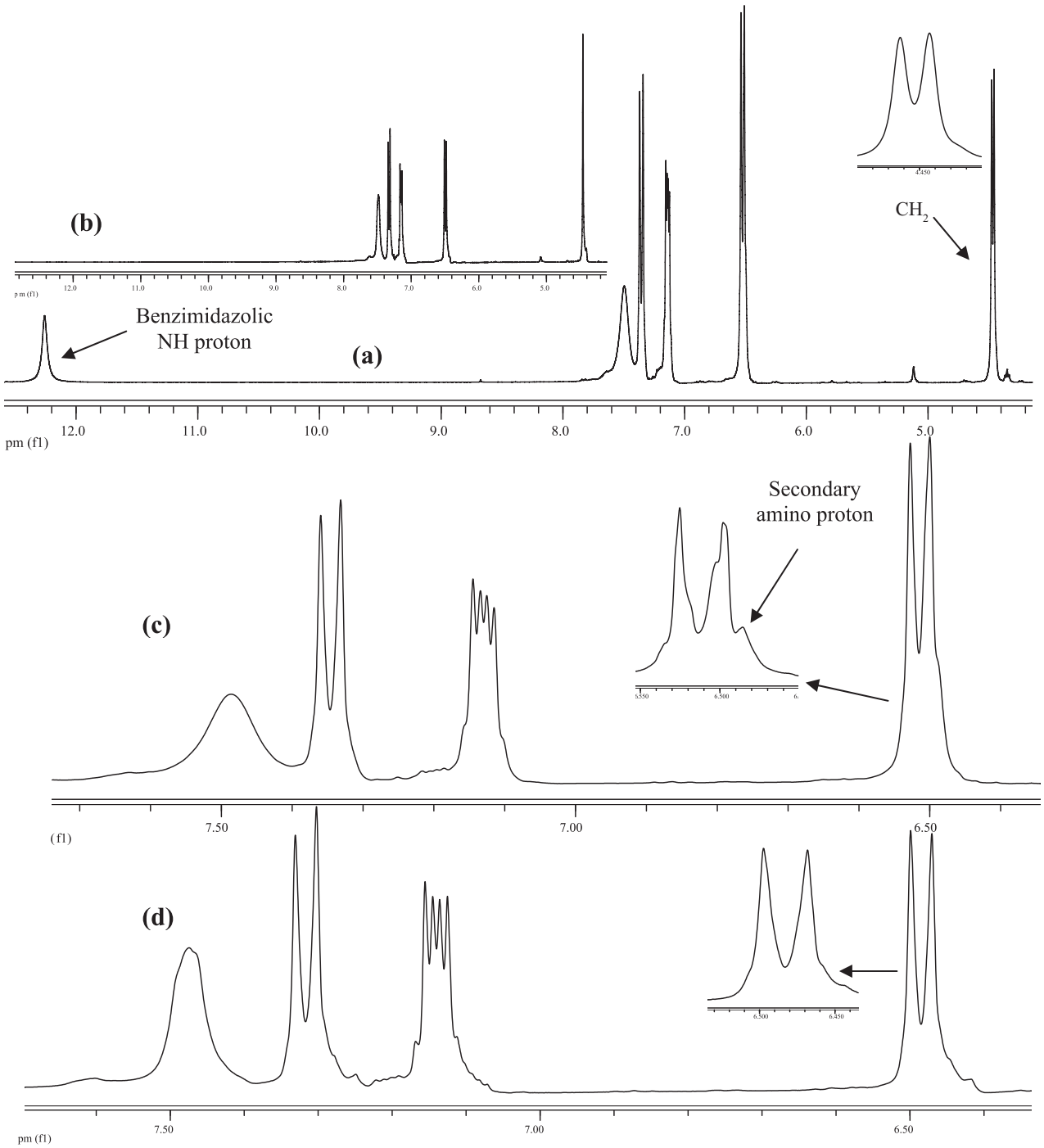

Fig. 4. (a) ^{1}H NMR spectrum of p-I derivative (L^2) in DMSO (b) ^{1}H NMR spectrum in DMSO/D_2O; (c) Aromatic region in DMSO (d) Aromatic region in DMSO/D_2O.

and 11.50 ± 0.01 for the benzimidazole (L^2) are assigned to the latter processes as p-Cl derivative. It was found that the ionization of the secondary amino group is directly influenced to some extent by both the type and nature of the substituents. Thus, the substituents of electron withdrawing characters increase the acidic behavior of the NH_{sec} group.

4. DFT studies

4.1. Geometry optimization

Full geometry optimizations of the title compounds were performed at the DFT level of theory [9]. Table 4 presents the optimized structure parameters of the benzimidazoles ($L^{1,2}$) as calculated by DFT/B3LYP level of theory using 6-31G (d) and SDD basis set, respectively. For L^1 derivative, a significant difference (0.067 Å) is found between the bond lengths N15—C7 and N16—C7. Similar, a difference of 0.064 Å is found between the latter bonds in the L^2 compound. This confirms that the hydrogen atom is fixed at one of the two nitrogen atoms through the intermolecular hydrogen bonding. Moreover, these bond lengths have a shorter distance than any amine compound due to the participation of the lone electron pair of the nitrogen atom in resonance of the benzimidazole ring. It is found that, the phenyl ring appears little distorted and its angles are slightly out of the perfect hexagonal structure. This is due to the attachment of the imidazole moiety to the benzene ring in the

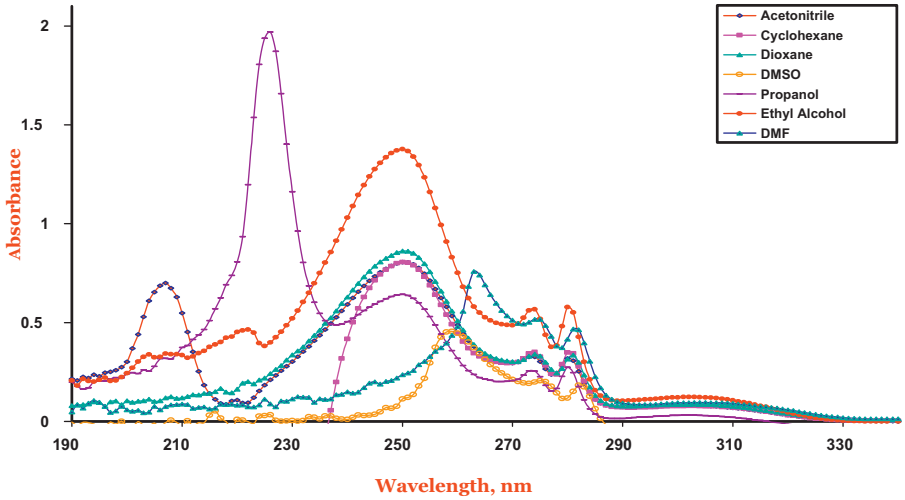

Fig. 5. Electronic absorption spectra of (3×10^{-5} M) of p-Cl (L^1) derivative in different solvents.

place of hydrogen atoms. The breakdown of hexagonal symmetry of the benzene ring in the p-Cl derivative is obvious from the elongation of C4—C5 (1.415 Å) and C1—C2 (1.409 Å) comparing to the remaining C1—C3, C3—C4, C2—C6 and C5—C6 bonds, which almost have the same bond lengths as will be confirmed latter by the NBO analysis.

Substitution in the para position of the aniline ring with halogen atom (X = Cl, and I) leads to some changes in the bond lengths and bond angles of the aniline moiety as a result of the charge redistribution. Due to the σ-withdrawing character of the halogen atom, the optimized C-C bond lengths adjacent to the halogen atom are slightly shorter than the corresponding ones in the unsubstituted derivative [30] at the same level of theory. In addition, the angle (C11—C12—C13) in L^1 or (C15—C16—C17) in L^2 near to the position of halogen is longer than that found in case of the unsubstituted compound [30]. The dipole moment of the unsubstituted derivative [30] increases dramatically from 3.615 D to 5.388 and 6.321 D for the chloro-, and iodo-derivatives, respectively. The high electronegativity of the halogen atom induces polarization both in σ- and π-frameworks of the aniline moiety. The studied compounds ($L^{1,2}$) show accumulation of the negative charge density on the pyridine-type nitrogen, which is a very important structural feature related directly to the ability to bind the metal ions. Several calculated thermodynamic parameters are presented in Table 4.

4.2. Natural bond orbital (NBO) analysis

The natural bond orbital (NBO) calculation [13] of $L^{1,2}$ compounds was performed using NBO 3.1 program implemented in the *GAUSSIAN03* package at the DFT/B3LYP level. The ideal Lewis structure picture is constructed from Lewis σ-type (donor) NBOs that are complemented by the non-Lewis σ-type (acceptor) NBOs. The filled NBOs of the natural Lewis structure are well adapted to describe covalency effects in molecules. The anti-bonds represent empty valence-shell capacity and spanning portions of the atomic valence space that are formally unsaturated by covalent electrons. Weak occupancies of the valence anti-bonds signal irreducible departure from an idealized localized Lewis picture, i.e. true "delocalization effects". Therefore, NBO analysis provides an efficient method for studying intra- and intermolecular bonding and provides a convenient basis for investigating charge transfer or conjugative interaction in molecular systems.

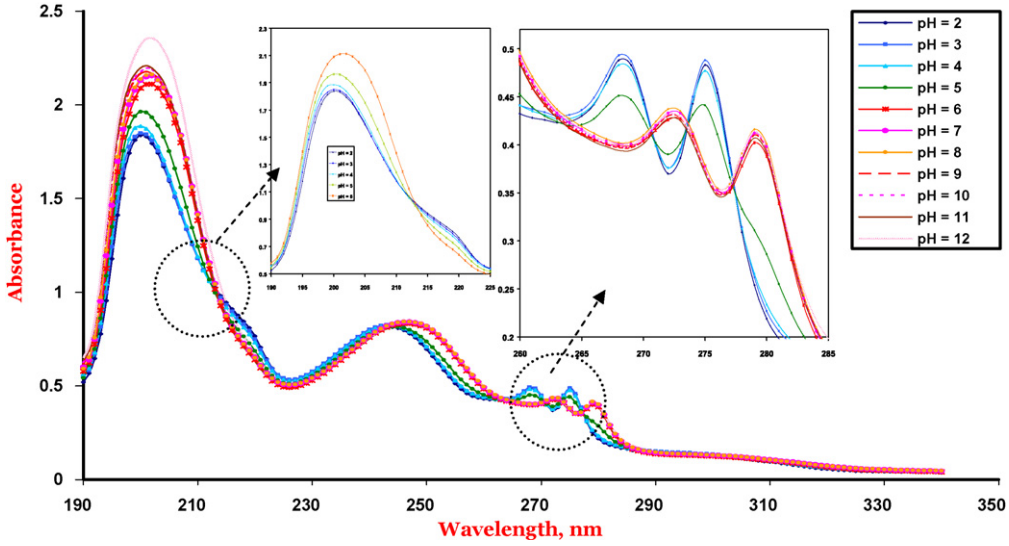

Fig. 6. Electronic absorption spectra of (3×10^{-5} M) of p-Cl derivative (L^1) in solutions of varying pH.

Table 4
Selected bond lengths (Å), angles (°) and charge for $L^{1,2}$ compounds.

L^1					L^2				
Bond lengths (Å)		Bond angles (°)		Charge	Bond lengths (Å)		Bond angles (°)		Charge
C1C2	1.409	C3C1C2	121.410	C1 = −0.143	C1C2	1.407	C1C2C3	117.858	C1 = −214
C1C3	1.391	C4C3C1	117.974	C2 = −0.148	C2C3	1.404	C2C3C4	121.336	C2 = −194
C3C4	1.399	C5C4C3	119.841	C3 = −0.178	C3C4	1.421	C3C4C5	121.547	C3 = −0.333
C4C5	1.415	C6C2C1	121.546	C4 = 0.239	C4C5	1.406	C4C5C6	116.719	C4 = 0.027
C5C6	1.395	C7N16C4	105.265	C5 = 0.354	C5C6	1.404	H7C2C1	120.454	C5 = 0.253
C4C7	2.147	C8C7N16	124.367	C6 = −0.174	C1C6	1.428	H8C3C2	119.577	C6 = −0.359
C7C8	1.502	N17C8C7	109.087	C7 = 0.515	C11C12	1.506	H9C4C3	119.169	C7 = 0.149
C8C9	2.474	C10C9N17	119.565	C8 = −0.171	C13C14	1.422	H10C5C4	121.016	C8 = −0.406
C9C10	1.410	C11C10C9	121.113	C9 = 0.372	C14C15	1.401	C1N21C11	105.806	C9 = 0.458
C10C11	1.389	C12C11C10	119.737	C10 = −0.186	C15C16	1.409	N21C11C12	123.415	C10 = −0.406
C11C12	1.396	C13C12C11	120.296	C11 = −0.135	C16C17	1.404	C11C12N22	108.619	C11 = -0.123
C12C13	1.391	C14C13C12	119.943	C12 = −0.073	C17C18	1.407	N22C13C14	148.335	C12 = −0.359
C13C14	1.395	C14C9C10	118.115	C13 = −0.141	I19C16	2.145	C13C14C15	121.035	C13 = −0.150
C9C14	1.407	N16C7N15	113.044	C14 = −0.180	N22C12	1.451	C14C15C16	119.929	C14 = −0.332
N15C7	1.376	C7N15C5	107.101	N15 = −0.747	N21C11	1.330	C15C16C17	120.056	N15 = −0.444
N16C7	1.309	N16C4C5	110.130	N16 = −0.576	N20C11	1.394	C16C17C18	120.098	N16 = −0.126
N17C9	1.385	N15C5C4	104.459	N17 = −0.682	N22C13	1.386	I19C16C15	119.773	N17 = −0.429
C12Cl18	1.764	H19C3C1	121.719	Cl = −0.045	H23N20	1.011	N20C11C12	123.415	I = 0.066
H23N15	1.010			H23 = 0.333	H26N22	1.016			H23 = 0.228
H26N17	1.014			H26 = 0.352					H26 = 0.347
E (a.u.)			−719.181			−716.280			
Zero-point *E* (kcal mol^{-1})			147.655			147.887			
Rotational constants (GHz)			1.932, 0.112, 0.106			1.957, 0.064, 0.062			
Entropy (cal mol^{-1} K^{-1})									
Translational			42.532			43.444			
Rotational			33.901			34.987			
Vibrational			48.777			50.495			
Total dipole moment (D)			5.388			6.321			

Hyperconjugation may be given as a stabilizing effect that arises from an overlap between an occupied orbital with another neighboring electron deficient orbital when these orbitals are properly oriented. The hyperconjugative interaction energy was deduced from the second-order perturbation approach of Fock Matrix in NBO basis between donor–acceptor orbitals [35]. The larger the second order interaction energy (E^2) value, the more intensive is the interaction between electron donors and electron acceptors, i.e. the more donating tendency from electron donors to electron acceptors and the greater the extent of conjugation of the whole system. These interactions can be identified by finding an increase in the electron density (ED) of the anti-bonding orbital that weakens the respective bonds. The results of NBO analysis for the p-Cl derivative show that the π(C2—C6) and π(C7—N16) participate as donor and the π*(C4—C5) anti-bond as acceptor, [π(C2—C6) → π*(C4—C5)] and [π(C7—N16) → π*(C4—C5)] with charge transfer energy values 280 and 340 J mol^{-1}, respectively. These interactions weaken the C4—C5 bond with elongation of its bond length as previously mentioned. The σ(C4—C5) is formed from $sp^{2.08}$ hybrid on C4 (which is a mixture of 32.43% s, and 67.52% p atomic orbitals) and $sp^{2.02}$ on C5 (66.90% p contribution) as shown in Table 5. Thus, the increasing of p characters on carbons C4 and C5 bond orbitals result in lengthening of the σ(C4—C5) bond than the other C—C bond lengths in the benzene ring of the benzimidazole moiety. In addition, the intramolecular hyperconjugative interaction of the π electrons occurs from C1—C3 to π*(C2—C6) (ED ≈ 0.335e and E^2 = 280 J mol^{-1}) leads to strong stabilization of the benzene ring of the benzimidazole moiety. The lone pair interaction of LP N16 ($sp^{2.12}$) with anti-bonding σ*(C7—N15) has a large energy difference (~810 J mol^{-1}) which is an evidence for charge transfer from nitrogen atom to the σ*(C7—N15) and induces partial π character. As shown in Table 5, p-I (L^2) derivative has the same behavior as the other derivative, where the strongest interaction is LP(1)N17 → π*(C9—C14) (ED ≈ 0.427e and E^2 = 44.7 kJ mol^{-1}).

4.3. Frontier molecular orbitals

The frontier molecular orbitals play an important role in the electric and optical properties [36]. The frontier orbital gap helps to characterize the chemical reactivity and kinetic stability of the molecule. A molecule with a small frontier orbital gap is more polarizable, is generally associated with a high chemical reactivity, low kinetic stability, and is termed as soft molecule. Fig. 7 shows the distributions and energy levels of the HOMO and LUMO orbitals for the studied compounds. The values of the energy separation between HOMO and LUMO are 4.71 and 4.38 eV for the benzimidazoles ($L^{1,2}$), respectively.

4.4. Electrochemical studies

The redox behavior of the benzimidazoles ($L^{1,2}$) was studied by cyclic voltammetry (CV) in acetonitrile in presence of $NaClO_4 \cdot H_2O$ as a supporting electrolyte. These compounds behave similarly and are oxidized in a two irreversible one-electron processes following the ECEC mechanism as shown in Fig. 8. The studied compounds form the cation-radical through a one-electron loss, which is followed by a deprotonation process from the imidazolic NH group to give the corresponding radical (Scheme 1). This radical undergoes the second electron transfer followed by the removal of another proton from the secondary amino group to form the di-radical [37]. In order to elucidate the effect of the introduction of the substituent (Cl and I) on the para-position of the aniline moiety, the CV of the unsubstituted derivative [30] has been also conducted. The unsubstituted derivative exhibited the oxidation processes at 0.93 and 1.27 V, while the p-Cl (L^1) derivative showed these processes at 0.98 and 1.44 V. Thus, the presence of chlorine substituent in the para-position of the aniline moiety shifts the second oxidation process towards higher potential. On the other hand, the p-I (L^2) derivative showed only the first oxidation process at 1.04 V.

Table 5
The most important interactions between "filled" (donors) Lewis-type NBOs and "empty" (acceptors) non-Lewis NBOs.

Donor[a] Lewis-type NBOs (A—B)	Occupancy	Hybrid[e]	AO (%)[f]	Acceptor[b] non Lewis NBOs	NBOs	E^2 (kJ mol^{-1})	$E(j)-E(i)^c \times 10^3$(kJ mol^{-1})	$F(i,j)^d \times 10^3$(kJ mol^{-1})
L^1								
π(C1—C3)	1.712	sp (C1) sp (C3)	s(0.00)p(99.96) s(0.00)p(99.95)	π*(C2—C6)	0.335	20.29	0.28	0.068
π(C2—C6)	1.724	sp (C2) sp (C6)	s(0.00)p(99.96) s(0.00)p(99.96)	π*(C4—C5)	0.473	20.06	0.28	0.070
π(C4—C5)	1.599	sp (C4) sp (C5)	s(0.00)p(99.97) s(0.00)p(99.97)	π*(C1—C3)	0.308	18.48	0.29	0.067
π(C7—N16)	1.878	sp (C7) sp (N16)	s(0.00)p(99.90) s(0.00)p(99.70)	π*(C4—C5)	0.473	17.73	0.34	0.077
π(C9—C14)	1.640	sp (C9) sp (C14)	s(0.01)p(99.95) s(0.00)p(99.97)	π*(C12—C13)	0.404	25.28	0.27	0.075
LP(1)N15	1.627	sp	s(0.00)p(99.98)	π*(C4—C5)	0.473	31.59	0.30	0.090
LP(1)N15	1.627	sp	s(0.00)p(99.98)	π*(C7—N16)	0.341	50.00	0.29	0.107
LP(1)N16	1.915	$sp^{2.12}$	s(32.00)p(67.85)	σ*(C7—N15)	0.042	10.43	0.81	0.083
LP(1)N17	1.783	$sp^{18.74}d^{0.01}$	s(5.06)p(94.91)d(0.03)	π*(C9—C14)	0.417	37.10	0.29	0.098
LP(1)Cl	1.993	$sp^{0.22}$	s(82.23)p(17.75)	π*(C12—C13)	0.405	10.98	0.33	0.059
L^2								
π(C4—C5)	1.602	sp (C4) sp (C5)	s(0.00)p(100.00) s(0.00)p(100.00)	π*(C1—C3)	0.304	19.56	0.29	0.069
π(C4—C5)	1.602	sp (C4) sp (C5)	s(0.00)p(100.00) s(0.00)p(100.00)	π*(C2—C6)	0.332	19.61	0.28	0.068
π(C9—C14)	1.971	sp (C9) sp (C14)	s(0.00)p(100.00) s(0.00)p(100.00)	π*(C12—C13)	0.403	27.69	0.27	0.079
π(C12—C13)	1.713	sp (C12) sp (C13)	s(0.00)p(100.00) s(0.00)p(100.00)	π*(C10—C11)	0.320	23.20	0.29	0.074
LP(1)N15	1.638	sp	s(0.00)p(100.00)	π*(C4—C5)	0.476	30.75	0.31	0.089
LP(1)N16	1.919	$sp^{1.98}$	s(33.59)p(66.41)	σ*(C7—N15)	0.044	10.35	0.74	0.079
LP(1)N17	1.760	sp	s(0.00)p(100.00)	π*(C9—C14)	0.427	44.70	0.27	0.103
LP(1)I	1.993	$sp^{0.12}$	s(89.33)p(10.67)	π*(C12—C13)	0.403	5.97	0.28	0.040

[a] LP(n)A is a valence lone pair orbital (n) on A atom.
[b] (*) denotes anti-bonding, and Ry corresponds to the Rydberg NBO orbital.
[c] Energy difference between donor and acceptor i and j NBO orbitals.
[d] $F(i, j)$ is the Fock matrix element between i and j NBO orbitals.
[e] Hybrid on A atom in the A—B bond or otherwise, as indicated.
[f] Percentage contribution of atomic orbitals in NBO hybrid.

The reduction of the investigated compounds ($L^{1,2}$) is done easily through the acceptance of two electrons in one irreversible two-electron-wave producing the corresponding dianion of the imine moiety, which is basic enough to accept two protons not only from the residual water, but also from the supporting electrolyte.

It might be tempting now to correlate the values E_{ox} derived from CV with HOMO–LUMO energy differences obtained from DFT calculations. The UV–vis absorption of a molecule corresponds indeed to excitation of an electron from the HOMO into the LUMO, whereas electro-oxidation corresponds only to the removal of an electron from the HOMO. A correlation might be possible if reduction of this molecule (i.e. donation of an electron into the LUMO) may be possible; in this case, the potential difference between oxidation and reduction potentials may be correlated with the HOMO–LUMO energy gap [38]. The potential difference between the first oxidation peaks in the unsubstituted derivative and that of the p-Cl derivative (L^1) is 0.06 V, which is in a good agreement with the shift, associated with the HOMO–LUMO gaps on going from the unsubstituted derivative to the p-Cl compound (0.06 eV) [6]. The DFT data have assigned that the LUMO of the p-Cl (L^1) and p-I (L^2) derivatives are constituted mainly by C=N group of the benzimidazole ring and thus the reduction is considered as electron accommodation at C=N dominated orbitals.

4.5. Biological activity

The antimicrobial activities of the studied compounds were carried out using cultures of *B. subtilis*, *S. aureus*, and *S. faecalis* as Gram-positive bacteria and *E. coli*, *P. aeruginosa*, and *N. gonorrhea* as Gram-negative bacteria and compared with those of the unsubstituted derivative, (1H-benzimidazol-2-ylmethyl)-*N*-phenyl amine [30]. In the earlier studies [30], it was found that, the unsubstituted derivative is more toxic than the standard tetracycline against the bacterium *S. aureus* with a minimum inhibitory concentration (58 μg/ml) as compared with tetracycline (82 μg/ml). As shown in Fig. 9, the title compounds have the capacity of inhibiting the metabolic growth of the investigated bacteria to different extents especially the *P. aeruginosa*, but less than the unsubstituted derivative. The toxicity of these compounds may be arising from the benzimidazole ring, which may play an important role in the antibacterial activity [6].

In classifying the antibacterial activity as Gram-positive or Gram-negative, it would be expected that a much greater number of drugs would be active against Gram-positive than Gram-negative bacteria [39]. However, in this study, the title compounds are active against both types of the bacteria, which may indicate broad-spectrum properties. It is seen that the activity of the title compounds is affected by the nature of the substituents on the

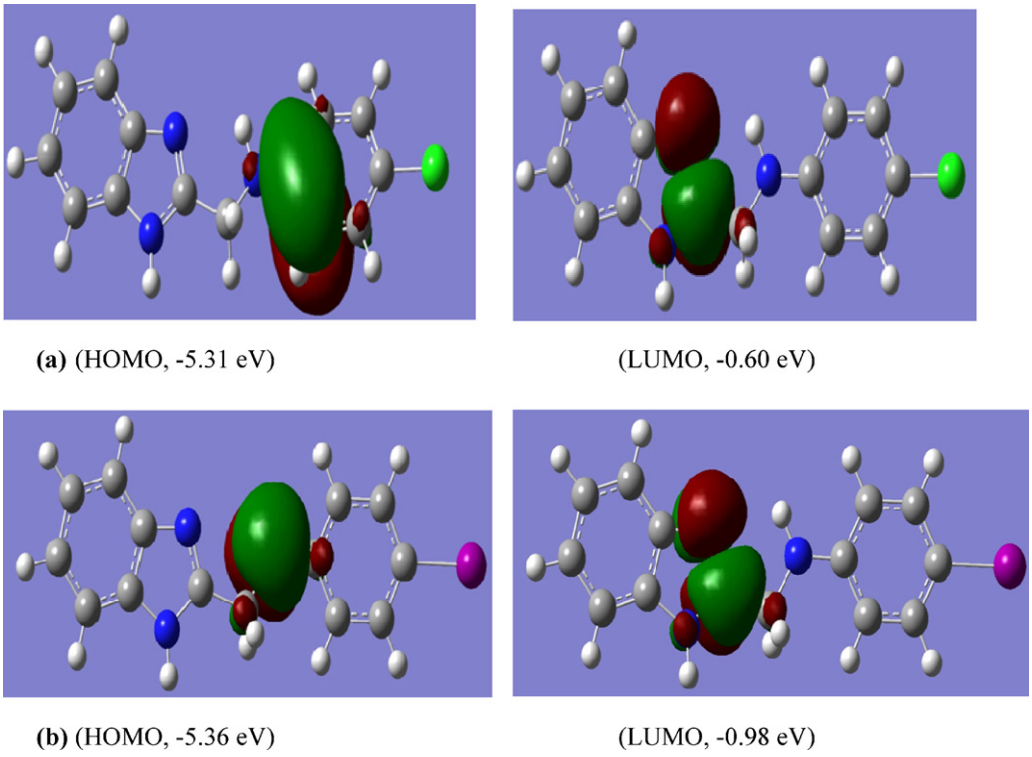

Fig. 7. Molecular orbital surfaces and energy levels of (a) p-Cl (L^1) and (b) p-I (L^2) derivatives.

aniline ring, this in relation to the lipophilicity of the compounds and their membrane permeability, a key factor in determining their entry inside the cells. The introduction of substituent (Cl or I) in the para-position of the aniline ring decreases markedly the antibacterial activity. The antibacterial effect declines on going from unsubstituted to p-Cl and finally p-I derivative. On the other hand, the variation in the effectiveness of the studied compounds against different organisms depends either on the impermeability

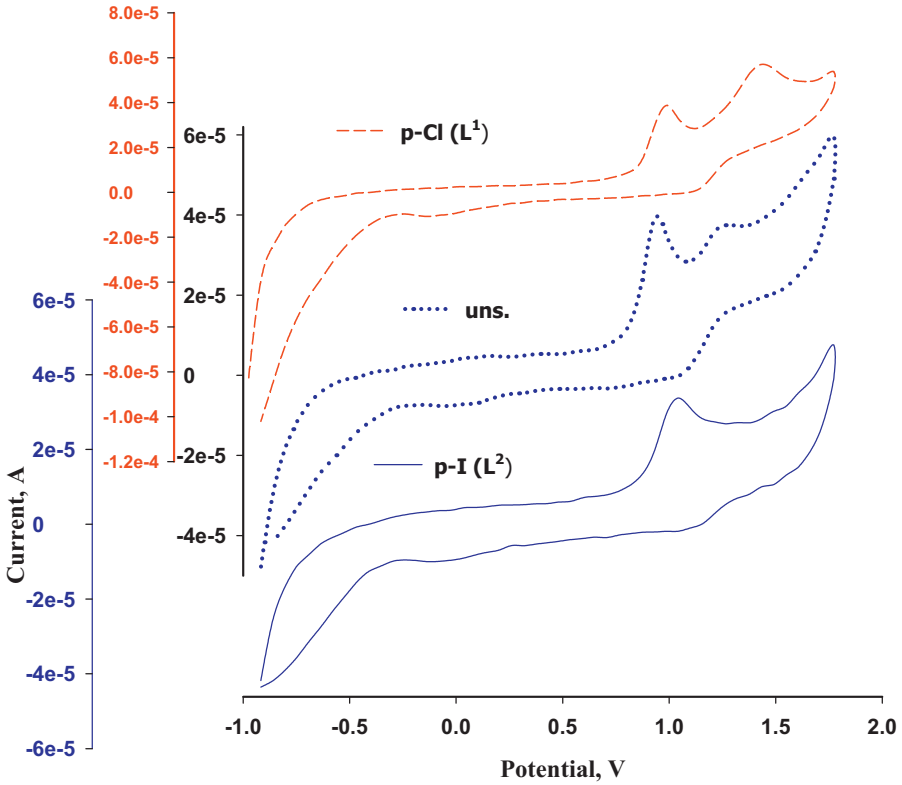

Fig. 8. CV of the benzimidazoles, p-Cl (L^1), p-I (L^2) and the unsubstituted derivative (uns.).

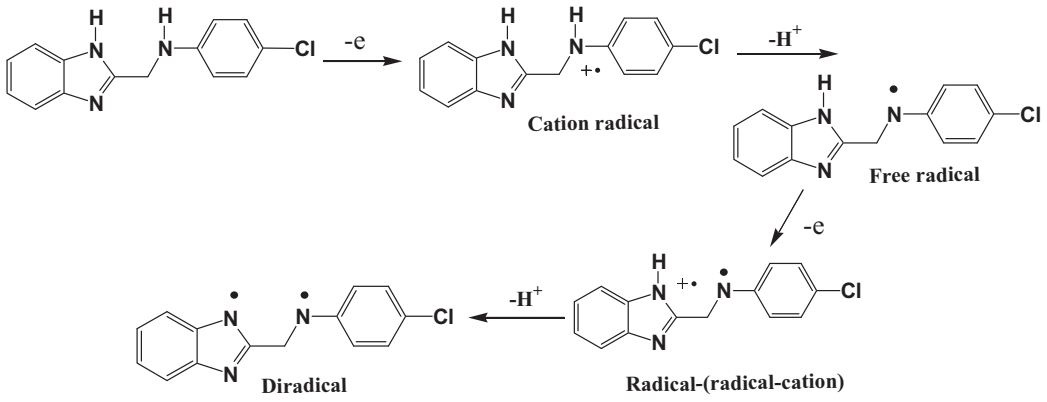

Scheme 1. Proposed oxidation mechanism for benzimidazole (L^1).

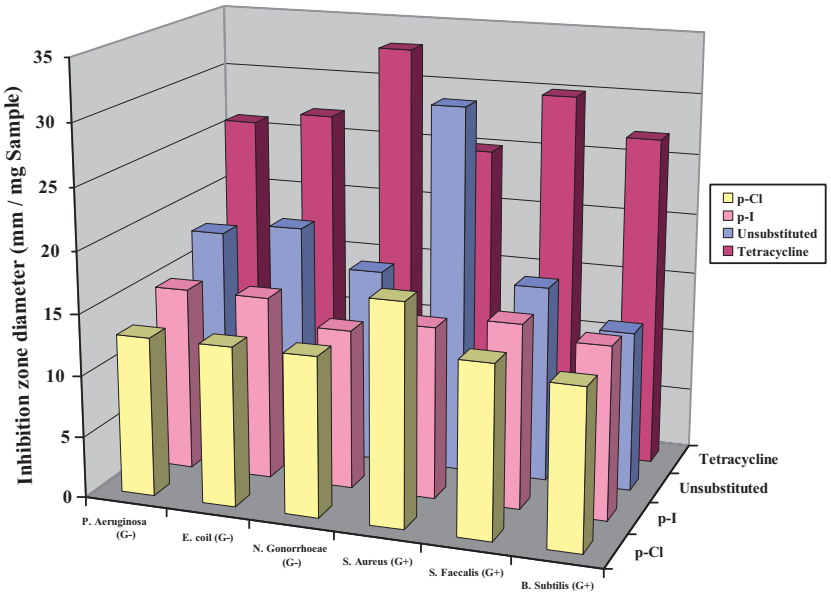

Fig. 9. Antibacterial activities of the benzimidazoles ($L^{1,2}$) and tetracycline against *B. subtilis*, *S. aureus*, and *S. faecalis* as Gram-positive, *P. aeruginosa*, *E. coli*, and *N. Gonorrhea* as Gram-negative bacteria. All experiments were carried out in triplicate and the mean results are given. DMSO was used as control and its inhibition zone was subtracting from that of each case.

of the cells of the microbes or on differences in ribosome of microbial cells.

5. Conclusion

In an effort to prepare new compounds with potential biological activity, we have synthesized and characterized (1H-benzimidazol-2-ylmethyl)-*N*-(4-chloro-phenyl)-amine (L^1) and (1H-benzimidazol-2-ylmethyl)-*N*-(4-iodo-phenyl)-amine (L^2) by spectral methods and elemental analysis. The PCM model fails to describe the experimental chemical shift associated with the NH protons and the specific solute-solvent interactions must be considered for a proper and reliable description of the influence of solvent on the chemical shifts associated with hydrogen-bonded systems. The specific solute-solvent interaction is the main controlling factor in determining the UV–vis band position. The electron-withdrawing substituents increase the acidic behavior of the NH_{sec} group. The high electronegativity of the halogen atom induces polarization both in σ- and π-frameworks of the aniline moiety. The title compounds have the capacity of inhibiting the metabolic growth of the investigated bacteria to different extents.

Appendix A. Supplementary data

Supplementary data associated with this article can be found, in the online version, at doi:10.1016/j.saa.2012.01.080.

References

[1] W.O. Foye, L.L. Thomas, A. David, B.I. Williams, Principles of Medicinal Chemistry, Waverly Pvt. Ltd., New Delhi, 1995.
[2] N.S. Pawar, D.S. Dalal, S.R. Shimpi, P.P. Mahulikar, Eur. J. Pharm. Sci. 21 (2004) 115–118.
[3] Y. He, J. Yang, B. Wu, L. Risen, E.E. Swayze, Bioorg. Med. Chem. Lett. 14 (2004) 1217–1220.
[4] İ. Ören, Ö. Temiz, İ. Yalcin, E. Şener, N. Altanlar, Eur. J. Pharm. Sci. 7 (1998) 153–160.
[5] T. Hisano, M. Ichikawa, K. Tsumoto, M. Tasaki, Chem. Pharm. Bull. 30 (1982) 2996–3004.
[6] (a) N.T. Abdel-Ghani, A.M. Mansour, J. Mol. Struct. 991 (2011) 108–126; (b) N.T. Abdel-Ghani, A.M. Mansour, Inorg. Chim. Acta 373 (2011) 249–258.
[7] N.T. Abdel-Ghani, A.M. Mansour, Spectrochim. Acta A 86 (2012) 605–613.
[8] N.T. Abdel-Ghani, A.M. Mansour, Spectrochim. Acta A 81 (2011) 754–763.
[9] (a) A.D. Becke, J. Chem. Phys. 98 (1993) 5648–5682; (b) C. Lee, W. Yang, R.G. Parr, Phys. Rev. B 37 (1998) 785–789.
[10] M.J. Frisch, G.W. Trucks, H.B. Schlegel, G.E. Scuseria, M.A. Robb, J.R. Cheeseman, V.G. Zakrzewski, J.A. Montgomery, R.E. Stratmann, J.C. Burant, S. Dapprich, J.M. Millam, A.D. Daniels, K.N. Kudin, M.C. Strain, O. Farkas, J. Tomasi, V. Barone,

M. Cossi, R. Cammi, B. Mennucci, C. Pomelli, C. Adamo, S. Clifford, J. Ochterski, G.A. Petersson, P.Y. Ayala, Q. Cui, K. Morokuma, D.K. Malick, A.D. Rabuck, K. Raghavachari, J.B. Foresman, J. Cioslowski, J.V. Ortiz, A.G. Baboul, B.B. Stefanov, G. Liu, A. Liashenko, P. Piskorz, I. Komaromi, R. Gomperts, R.L. Martin, D.J. Fox, T. Keith, M.A. Al-Laham, C.Y. Peng, A. Nanayakkara, C. Gonzalez, M. Challacombe, P.M.W. Gill, B.G. Johnson, W. Chen, M.W. Wong, J.L. Andres, M. Head-Gordon, E.S. Replogle, J.A. Pople, GAUSSIAN 03 (Revision A.9), Gaussian, Inc., Pittsburgh, 2003.

[11] A. Frisch, A.B. Nielson, A.J. Holder, GAUSSVIEW User Manual, Gaussian Inc., Pittsburgh, PA, 2000.

[12] Recent developments and applications of modern density functional theory, in: M.E. Casida, J.M. Seminario (Eds.), in: Theoretical and Computational Chemistry, vol. 4, Elsevier, Amsterdam, 1996, p. 391.

[13] F. Weinhold, J.E. Carpenter, The Structure of Small Molecules and Ions, Plenum, New York, 1988, p. 227.

[14] R. Ditchfield, Chem. Phys. 76 (1972) 5688–5691.

[15] M.I. Rahman, W.J. Choudhary, Thomsen, Bioassay Techniques for Drug Development, Harwood Academic Publishers, The Netherlands, 2001, p. 16.

[16] National Committee for Clinical Laboratory Standards, NCCLS Approval Standard Document M2-A7, Vilanova, PA, 2000.

[17] A. Rahman, M.I. Choudhary, W.J. Thomsen, Bioassay Techniques for Drug Development, Harwood Academic Publishers, Netherlands, 2001, p. 16.

[18] (a) G. Rauhut, P. Pulay, J. Phys. Chem. 99 (1995) 3093–3100;
(b) J.A. Pople, H.B. Schlegel, R. Krishnan, J.S. Defrees, J.S. Binkley, M.J. Frisch, R.A. Whiteside, Int. J. Quantum Chem.: Quantum Chem. Symp. 15 (1981) 269–278.

[19] (a) M.W. Ellzy, J.O. Jensen, H.F. Hameka, J.G. Kay, D. Zeroka, Spectrochim. Acta 57A (2001) 2417–2432;
(b) J.O. Jensen, A. Banerjee, C.N. Merrow, D. Zeroka, J.M. Lochner, J. Mol. Struct.: Theochem. 531 (2000), 323–231;
(c) J.O. Jensen, D. Zeroka, J. Mol. Struct.: Theochem. 487 (1999) 267–274.

[20] K. Hofmann, Imidazole and its Derivatives, Interscience Publishers, New York, 1953.

[21] (a) S. Mohan, N. Sundaraganesan, Spectrochim. Acta A 47 (1991) 1111;
(b) N. Sundarag-anesan, S. Ilakiamani, P. Subramani, B. Dominic Joshua, Spectrochim. Acta A 67 (2007) 628–635.

[22] N.M. Agathabay, M. Tulu, M. Somer, D. Haciu, A. Yilmaz, Struct. Chem. 19 (2008) 21.

[23] F.S. Miranda, F.G. Menezes, J. Vicente, A.J. Bortoluzzi, C. Zucco, A. Neves, N.S. Gonçalves, J. Mol. Struct. 938 (2009) 1–9.

[24] S. Sebastian, N. Sundaraganesan, Spectrochim. Acta A 75 (2010) 941–952.

[25] (a) S. Miertus, E. Scrocco, J. Tomasi, Chem. Phys. 55 (1981) 117;
(b) R. Cammi, J. Tomasi, J. Comput. Chem. 16 (1995) 1449.

[26] V. Chiş, A. Pîrnău, M. Vasilescu, R.A. Varga, O. Oniga, J. Mol. Struct. (Theochem.) 851 (2008) 63–74.

[27] R.M. Issa, A.A. Hassanein, I.M.R.I. El-Mehasseb, A. El-Wadoud, Spectrochim. Acta Part A 65 (2006) 206–214.

[28] (a) M. Krishnamurthy, P. Phaniraj, S.K. Dogra, J. Chem. Soc. Perkin Trans. II (1986) 1917–1925 (and the references therein);
(b) A.K. Mishra, S.K. Dogra, J. Photochem. 31 (1985) 333–344; Indian J. Phys., Sect. B 54 (1984) 480; Spectrochim. Acta. Part A, 39 (1983) 609–615.

[29] R.M. Issa, S.A. El-Daly, N.A. El-Wakiel, Spectrochim. Acta Part A 59 (2003) 723–728.

[30] N.T. Abdel-Ghani, A.M. Mansour, Spectrochim. Acta A 81 (2011) 529–543.

[31] P.N. Preston, Benzimidazoles and Congeneric Tricyclic Compounds, Part I, Wiley, New York, 1981, p. 64.

[32] N.M. O'Boyle, GAUSSSUM 2.0, (2006), available from <http://gausssum.sf.net>.

[33] I.M. Issa, R.M. Issa, M.S. El-Ezaby, Y.Z. Ahemed, Z. Physik. Chem. 242 (1969) 169; I.M. Issa, R.M. Issa, M.S. El-Ezaby, Y.Z. Ahemed, Z. Physik. Chem. 250 (1972) 161.

[34] A.K. Mishra, S.K. Dogra, Bull. Chem. Soc. Jpn. 58 (1985) 3587;
A.K. Mishra, S.K. Dogra, J. Photochem. 31 (1985) 333;
A.K. Mishra, S.K. Dogra, Indian J. Phys. Sect. B 54 (1984) 480;
A.K. Mishra, S.K. Dogra, Spectrochim. Acta Part A 39 (1983) 609.

[35] C. Ravikumar, I. Hubert Joe, V.S. Jayakumar, Chem. Phys. Lett. 460 (2008) 552–558.

[36] I. Fleming, Frontier Orbitals and Organic Chemical Reactions, Wiley, London, 1976.

[37] G.M. Abou-Elenien, A.A. El-Maghrdy, H.R. Abdel-Twab, Electroanalysis 13 (7) (2001) 587–595.

[38] M. Al-Anber, B. Milde, W. Alhalasah, H. Lang, R. Holze, Electrochim. Acta 53 (2008) 6038–6047.

[39] A.R. Mcutcheon, S.M. Ellis, R.E.W. Hancock, G.H.N. Towers, J. Ethnopharmacol. 37 (1992) 213–223.